A numerical study on using guided GPR waves along metallic cylinders in boreholes for permittivity sounding

Pre-reviewed version

Sam Stadler[1] Jan Igel[2]
Leibniz Institute of Applied Geophysics
Stilleweg 2, 30655 Hannover, Germany

Email: [1]Sam.Stadler@leibniz-liag.de [2]Jan.Igel@leibniz-liag.de

***Abstract*—We performed a numerical study on using guided ground-penetrating radar (GPR) waves in boreholes for permittivity soundings using finite-difference (FDTD) simulations. The method presented here uses a GPR antenna that is placed next to a borehole in which a metal waveguide is lowered. Electromagnetic (EM) signals that the antenna sends out on the surface, couple to the waveguide and are reflected from the bottom end of the metal waveguide. Analysing the traveltimes yields accurate vertical distributions of the wave velocity, permittivity and water content in specified depth intervals. We performed numerical studies of the field distribution around the waveguide, the influence of the plastic borehole casing, as well as the resolution capabilites of the method in layered media. In this study, as a source, the GPR signal is introduced in the simulation via a 3D model of a real 400 MHz bowtie GPR antenna. We replicated the essential components of the antenna, e.g. the antenna bowties and metal casing, to accurately reproduce the transmitted signal. The guided wave has a skin depth drop in amplitude away from the waveguide of about 4.1 cm. Furthermore a maximum vertical resolution of high-contrast permittivity layers of about 5 cm is possible, and a formula for correcting the effect of the borehole casing on permittivity calculations is derived. We envision that this method and the insight from this study enables more precise soil soundings than other established GPR methods or time-domain reflectometry (TDR).**

***Index Terms*—Ground penetrating radar, Computational electromagnetics, Electromagnetic modeling, Finite difference methods, Electromagnetic fields, Time-domain analysis, Geophysical measurement techniques, Permittivity, Soil moisture**

I. Introduction

Knowledge of the water content distribution in the soil and vadose zone plays a key role for studying and understanding hydrological processes. Using geophysical methods to gain knowledge of the water-content distribution in the soil and vadose zone has gained more attention in the past years. Besides time-domain reflectometry (TDR) [1] being a fast, practicable and established method in determining water content , ground-penetrating radar (GPR) is gaining popularity for this purpose [2], [3]. GPR allows to estimate the permittivity of the ground via the electromagnetic (EM) wave velocity. Through petrophysical relations between the permittivity and the water content of a medium [3]–[5], the latter can be calculated. The accompanying velocity information is furthermore important for GPR when migrating data or performing time-depth-conversions.

Unguided EM waves in the ground exhibit a more complicated behaviour than waves guided by a TDR sensor [6]. We are proposing a new method to analyse the ground's permittivity by merging GPR and TDR and obtaining a greater vertical accuracy than either. By guiding GPR waves along a borehole and measuring its reflection, velocities and thereby permittivities in intervals of centimeter size, can be calculated.

Multiple aspects of this new method are yet unknown and difficult to determine in experiments. GPR has been studied through forward modeling tools in the past [7], and especially the recent advances of numerical software tools like gprMax [8] have proven to accurately simulate GPR problems. We present numerical studies about guided GPR waves in boreholes, namely the analysis

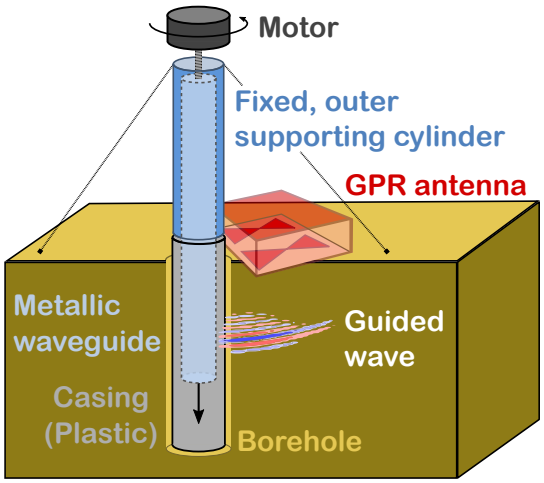

Fig. 1. Sketch of the guided GPR waves methodology.

of: its field distribution and sensing volume, its vertical resolution and the influence of a plastic borehole casing on the deduced permittivity.

II. The Guided-Waves Method

The core aspect of the Guided-Waves (GW) Method is determining phase velocities v in the ground through travel-time picking of GPR signals [9], [10]. When inserting a metal cylinder inside a borehole and placing a GPR antenna next to it, the GPR signal couples to the cylinder and a reflection from its lower end can be recorded, see Fig. 1. The early work of Sommerfeld [11] showed that electromagnetic waves that travel along a conducting cylinder/wire, travel at nearly the velocity of the surrounding material. There it was shown that an electromagnetic wave with a frequency of 1 GHz traveling along a copper wire with 4 mm radius, contains a phase velocity v error of about $3 \cdot 10^{-5}$ %. In addition, waveguides with greater radii reduce the error further, leading to the conclusion that the guided GPR waves used in this study have a negligible velocity difference to the surrounding material. This allows to conclude that the guided GPR waves presented here can be used to accurately determine v-distributions in the ground.

By lowering/raising the metal cylinder by a desired interval Δz, signal reflections at known depths are produced and allow for the following calculation of v via the depth of the cylinder z and the two-way traveltime t_{tw}:

$$v = \frac{2z}{t_{tw}} \approx \frac{c_0}{\sqrt{\varepsilon_r}} \tag{1}$$

The second part of eq. (1) states the relationship between the phase velocity and the relative permittivity ε_r, when assuming a non-magnetizable medium. An interval velocity v_i, denoted with subscript i, corresponding to only a specified depth interval Δz in the ground can be obtained by the difference of the travel-times from the upper and lower end of the interval:

$$v_i = \frac{2\Delta z}{t_{tw}(z_0 + \Delta z) - t_{tw}(z_0)} \approx \frac{c_0}{\sqrt{\varepsilon_{r,i}}} \tag{2}$$

By using (2), this method yields a detailed velocity/permittivity distribution of the underground.

We have developed a system that comprises two cylinders, an inner and an outer, as well as a motor, see the schematic in Fig.1. The outer cylinder is positioned on top of the borehole and serves to stabilize/guide the inner cylinder inside the borehole. The motor sits on top of the outer cylinder and is controlled to lower/raise the waveguide, the inner cylinder, inside the borehole.

The current apparatus has an inner cylinder with a diameter of $\approx$ 4.2 cm that fits exactly in the borehole casing made of a non-conducting standard PET material.

Figure 2 depicts a processed radargram of a measurement with guided GPR waves in a ground which has a strong permittivity contrast between an overlaying sand and a high permittivity peat layer at around 1.5 m depth. The water table is depicted in blue. One can clearly recognize the guided wave reflected at the bottom of the metallic cylinder.

III. Numerical Studies

A. Building a 3D antenna model

The GW Method consists of a metal cylinder that is in very close proximity to the GPR antenna and thereby in its reactive near-field. Including, or accounting for the coupling effects and interaction of the two should ensure a more accurate representation. This is why we opted to build a numerical model of the 400 MHz antenna that is used for the measurements, using the FDTD software gprMax [8]. The antenna model was designed to produce and transmit a signal as close to the real signal as possible. We built the numerical model using gprMax's internal geometry building tools, see Fig. 3. The remaining electric parameters of the materials inside the antenna were found via an optimization technique called taguchi's method [12], which is also available in gprMax [13].

B. Field distribution & sensing volume

In the first study we looked at the electromagnetic field distribution and sensing volume of the method around the metallic waveguide. We created a basic

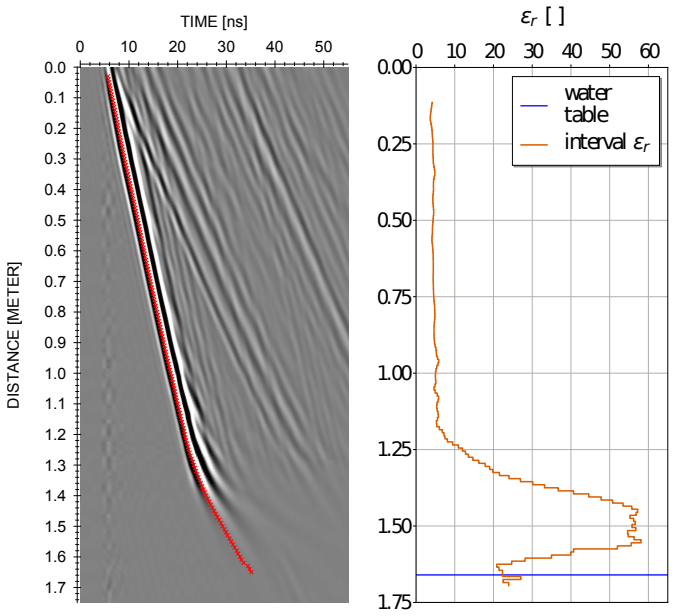

Fig. 2. Left: processed radargram of field data with a picked zero crossing phase (red) of the guided wave. Right: corresponding permittivities calculated from the travel-times in the intervals (orange), water table (blue).

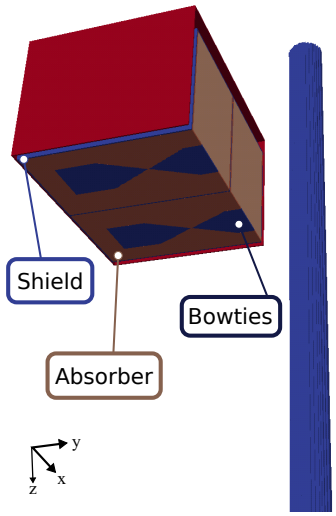

Fig. 3. View of the numerical 400 MHz antenna model, albeit truncated at two sides to allow to see the inside structures, and the metal cylindrical waveguide. The metallic case and bow-ties were modelled as perfect electric conductors.

numerical model with an air/ground interface on which the antenna is placed, and next to which a metallic waveguide/cylinder is inserted. Our initial model had a ground permittivity of $\varepsilon_r = 6$ and serves to illustrate the problem; the results are shown in Fig. 4. One can see that travelling downwards, the transmitted signal couples to the cylinder but is superimposed with the primary free space/spherical wave of the antenna. Only after the reflection from the cylinder's bottom end does the guided wave become isolated and clearly visible. A horizontal snapshot through the first amplitude maximum shows that the field y-component is distributed anti-symmetrically around the cylinder with a clear amplitude drop away from the cylinder. We simulated the same problem with four different ground permittivities spanning the typical range that can be found in soils, and the guided wave exhibited the same principal behaviour. By taking horizontal snapshots in three different depths the amplitude drop can be closer looked at. Figure 5 shows the amplitude drop with distance away from the cylinder, at different depths and in media with different permittivities. Only the amplitude drop on one side of the cylinder is shown because the signal is symmetric around the waveguide. More importantly though, away from the cylinders surface, the amplitude of all curves and in all media, drops to its skin depth at a distance of about 4.1 cm.

C. Guided waves in layered media

The second study focuses on the vertical resolution of an interface of two media with contrasting permittivities. We used a similar model as in section III-B, but introduced a layer with $\varepsilon_r = 20$ within a soil of $\varepsilon_r = 3$. What is clear beforehand is that the horizontal permittivity contrast will lead to a reflection which will be superimposed over the guided-wave reflection and cause some disturbances. The waveguide is extended vertically with 1 cm intervals to conform to the real measurement setup. The following processing methods will be used and compared to obtain a reliable set that yields the most accurate vertical resolutions: background removal, subtracting average, and calculating velocities over different depth intervals. The latter means that although a simulation is performed every 1 cm, the velocity is calculated over a greater interval than that to reduce the velocity error.

Figure 6 shows the radargrams of the raw data and a couple of processing results with the picked traveltimes. The raw radargram clearly shows the antenna crosstalk and reflections from the layer interfaces as vertical lines,

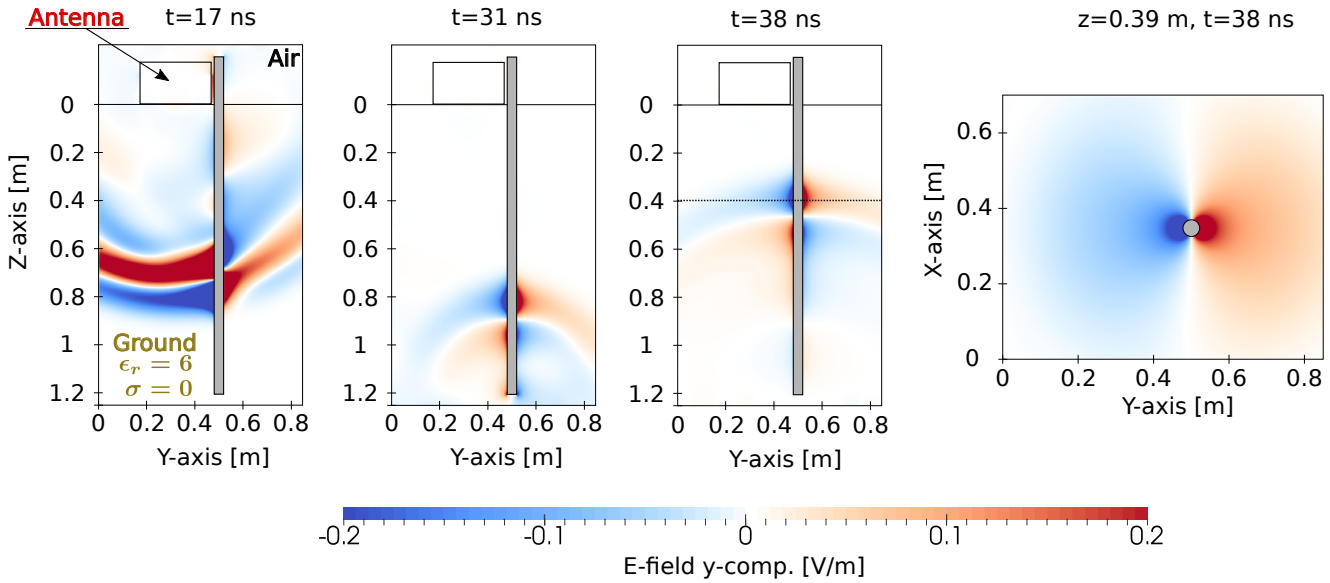

Fig. 4. Electric field distribution in the ground and around the metallic waveguide. The first three images show a vertical 2D slice through the middle of the antenna as well as the cylinder. The fourth image shows the horizontal distribution around the waveguide at $z = 0.39$ m, indicated by the black dottet line in the third image.

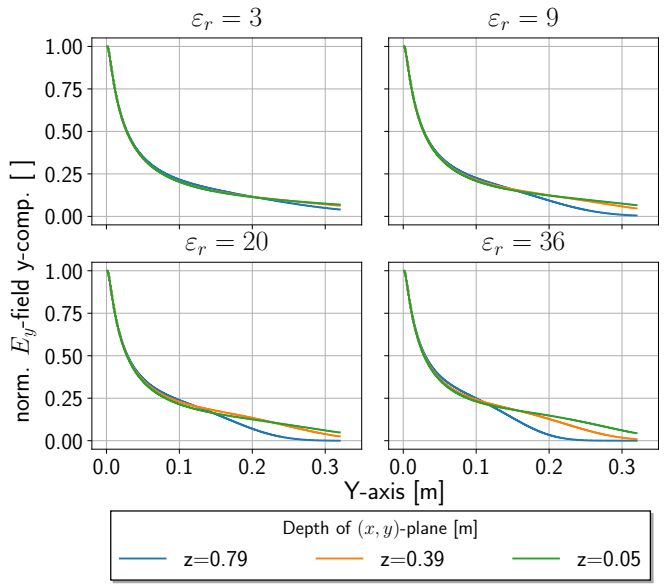

Fig. 5. Normalized electric field y-component amplitude with distance to the cylinder surface.

as well as the guided wave cutting diagonally through them. The background removal fails to completely get rid of the layer reflections, while subtracting the last trace or applying a moving average of 10 traces manages to remove them at least before the guided wave reflection begins. Although the last two techniques yield visually appealing radargrams with clear guided wave reflections, the derived interval velocities and permittivities will reveal how all techniques influence the picked traveltimes.

Figure 7 shows the best results of the different processing techniques on the picked traveltimes with the model shown in the background in gray. The subtracting average filter is shown with a window of 10 traces because that is where it performed best. All parameters are calculated over a 4 cm interval as that provides a clearer image at the layer interfaces. Filtering the data by subtracting the last trace and subtracting an average of 10 traces resolved the layer interfaces more accurately than the background removal. The latter is also the only one that does not yield correct permittivities in the intermediate layer.

D. Influence of plastic borehole casing

In the third study we look at the influence of a 1 mm plastic borehole casing, with $\varepsilon_r = 3$, on permittivity measurements. We already discussed the necessity of the plastic casing in section II, by comparing simulations with and without it in media with different permittivities, the impact shall become clear. Again, a similar model as in section III-B is used for the simulations, however the waveguide was placed 50 cm deep and a 1 mm thick plastic coating around the waveguide is included, for the latter see Fig. 8. It is expected that the coating will lead to reduced apparent calculated permittivities.

Figure 9 shows the results deduced from the picked traveltimes of the simulations with guided wave reflections. The black dots are the derived permittivities

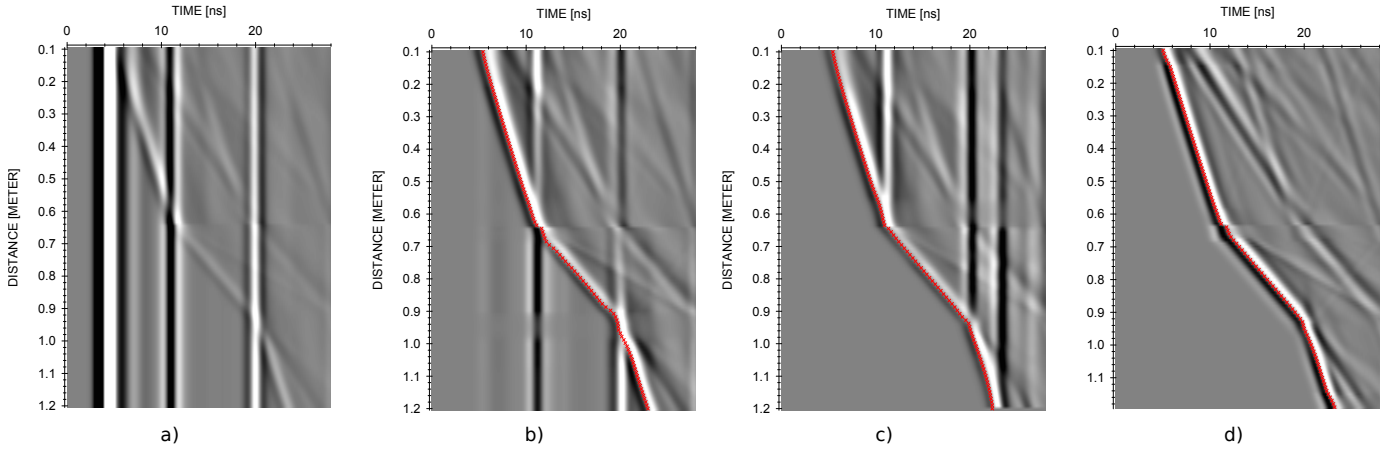

Fig. 6. Radargrams of the guided waves in layered media after applying different processing techniques, with the picks shown in red. a) raw radargram, b) background removal, c) subtracting the last trace, d) subtracting a moving average of 10 traces.

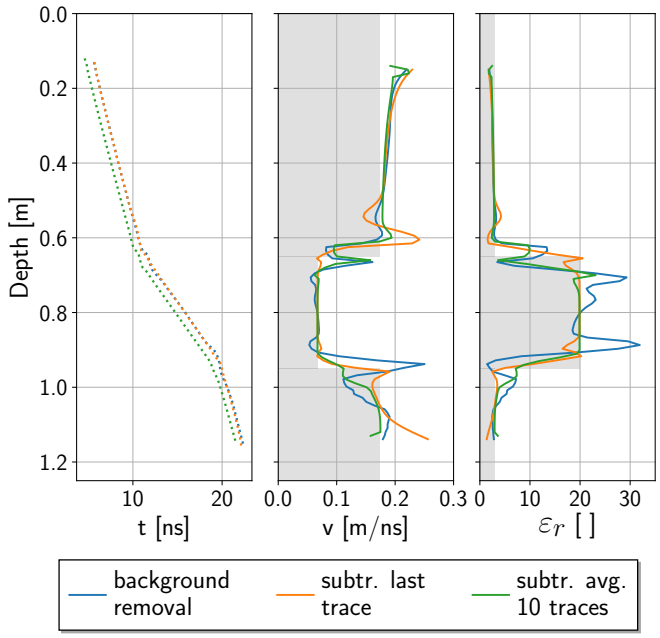

Fig. 7. Derived parameters from a simulation of guided waves in layered media, with the layer parameters depicted in gray. The waveguide was lowered with a 1 cm step, but the velocities and permittivities are calculated over a 4 cm interval.

from the simulations, which are fitted with a simple exponential function in green. The red dotted 1:1 line is the where the derived permittivities should land as it represents the value assigned to the media beforehand. The calculated permittivities are then corrected, blue dots, to the 1:1 line via a correction function which is depicted in the diagram.

It becomes clear that the influence is small for permittivities lower than 10, but becomes larger at higher

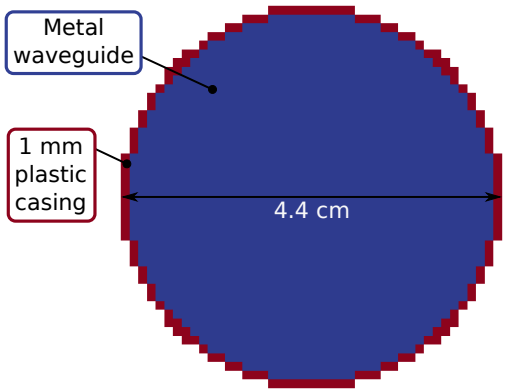

Fig. 8. Cross section of the metal cylinder with the 1 mm thick plastic coating.

permittivities. The results show that when using a measurement apparatus such as here with a plastic coating of 1 mm, the resulting permittivities from the interval velocities are reduced, but can be corrected for.

IV. Conclusion

The numerical studies presented here show some of the core aspects of using GPR waves guided along metallic cylinders in boreholes. The electric field y-component of the guided wave is distributed anti-symetrically around the waveguide and has a sensing volume of $\approx$ 4.1 cm. Concerning the vertical spatial resolution of the method, the simulations have shown that strong permittitivity contrasts may be resolved with up to 5 cm and that the permittivity of the medium can very well be resolved. To obtain the clearest image of the guided wave, it is recommended to filter the data by subtracting the last trace or use a subtracting

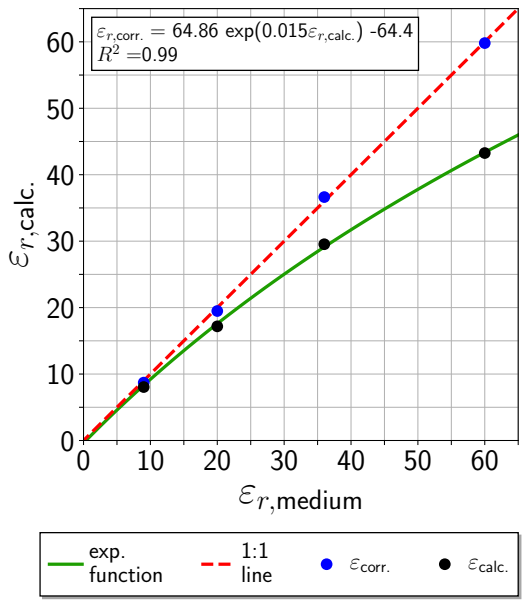

Fig. 9. Input and measured apparent permittivities, with the theoretical outcome lying on the red 1:1 line. The black dots depict the calculated permittivities in different media and under the influence of a plastic coating with a thickness of 1 mm. These are fitted with the green curves and corrected (blue dots) to the 1:1 line via the equation in the diagram.

average window of about 10 traces. Further study of the processing techniques with measured data shall provide more insight on this matter. Lastly, the influence of a plastic borehole casing proves to be strong in depths of about 50 cm and for permittivities greater than 10, and must be considered when analysing the data.

References

[1] D. A. Robinson, S. B. Jones, J. M. Wraith, D. Or, and S. P. Friedman., "A review of advances in dielectric and electrical conductivity measurements in soils using time domain reflectometry," *Vadose Zone Journal*, 2003.

[2] I. A. Lunt, S. S. Hubbard, and Y. Rubin, "Soil moisture content estimation using ground-penetrating radar reflection data," *Journal of Hydrology*, no. 307, pp. 254–269, 2005.

[3] H. Vereecken, J. A. Huisman, H. Bogena, J. Vanderborg, J. A. Vrugt, and J. W. Hopmans, "On the value of soil moisture measurements in vadose zone hydrology: A review," *Water Resources Research*, vol. 44, 2008.

[4] G. C. Topp, J. L. Davis, and A. P. Annan, "Electromagnetic Determination of Soil Water Content: Measurements in Coaxial Transmission Lines," *Water Resources Research*, vol. 16, no. 3, pp. 574–582, 6 1980.

[5] J. R. Birchak, C. G. Gardner, J. E. Hipp, and J. M. Victor, "High dielectric constant microwave probes for sensing soil moisture," *Proceedings of the IEEE*, vol. 62, pp. 93–98, 1974.

[6] J. A. Huisman, S. S. Hubbard, J. D. Redman, and A. Annan, "Measuring Soil Water Content with Ground Penetrating Radar: A Review," *Vadose Zone Journal*, vol. 2, no. 4, pp. 476–491, 2003.

[7] L. R. Roberts and J. J. Daniels, "Modeling near-field GPR in three dimensions using the FDTD method," *Geophysics*, vol. 62, no. 4, pp. 1114–1126, 1997.

[8] C. Warren, A. Giannopoulos, and G. Iraklis, "gprMax: Open source software to simulate electromagnetic wave propagation for Ground Penetrating Radar," *Computer Physics Communications*, 2016.

[9] J. Igel, H. Anschütz, J. Schmalholz, H. Wilhelm, W. Breh, H. Hötzl, and C. Hübner, "Methods for determining soil moisture with ground penetrating radar (GPR)," in *Field Screening Europe 2001.*, W. Breh, J. Gottlieb, H. Hötzl, F. Kern, T. Liesch, and R. e. Niessner, Eds. Springer, Dordrecht, 2001, pp. 484–491.

[10] J. Igel, S. Stadler, and T. Günther, "High-Resolution Investigation of the Capillary Transition Zone and its Influence on GPR Signatures," in *Proceedings of the 16th International Conference of Ground Penetrating Radar*, 2016.

[11] A. Sommerfeld, "Über die Fortpflanzung elektrodynamischer Wellen längs eines Drahtes," *Annalen Der Physik und Chemie*, vol. 67, no. 2, pp. 233–290, 1899.

[12] W. C. Weng, F. Yang, and A. Elsherbeni, "Electromagnetics and Antenna Optimization using Taguchi's Method," in *Synthesis Lectures on Computational Electromagnetics*. Morgan & Claypool, 2007, pp. 1–94.

[13] C. Warren and A. Giannopoulos, "Creating FDTD models of commercial GPR antennas using Taguchi's optimisation method," in *Proceedings of the 5th International Conference on Advanced Ground Penetrating Radar*, 2011.